Phase structure and monopoles in U(1) gauge theory

Werner Kerler
Fachbereich Physik, Universität Marburg, D-35032 Marburg, Germany

Claudio Rebbi
Department of Physics, Boston University, Boston, Massachusetts 02215

Andreas Weber
Fachbereich Physik, Universität Marburg, D-35032 Marburg, Germany
(Received 30 March 1994)

We investigate the phase structure of pure compact U(1) lattice gauge theory in four dimensions with the Wilson action supplemented by a monopole term. To overcome the suppression of transitions between the phases in the simulations we make the monopole coupling a dynamical variable. We determine the phase diagram and find that the strength of the first-order transition decreases with the increasing weight of the monopole term, the transition thus ultimately reaching second order. After outlining the appropriate topological characterization of networks of currents lines, we present an analysis of the occurring monopole currents which shows that the phases are related to topological properties.

PACS number(s): 11.15.Ha, 05.50.+q, 64.60.Fr

I. INTRODUCTION

The investigation of the phase structure of U(1) lattice gauge theory is important in two respects. First, the theory should be the basis of QED which is still not understood at the nonperturbative level. Second, it provides a unique model to study the interrelation between phase structure and topological properties of the field configurations.

The phase transition in four-dimensional (4D) compact U(1) lattice gauge theory is known to be related to the occurrence of monopoles. Using the formulation of DeGrand and Toussaint [1], Barber *et al.* have shown that, if one adds a monopole term to the action, depending on its weight the transition can be suppressed [2] or shifted [3]. The consequences of removing monopoles in the U(1) theory have also been studied in [4].

Recent results [5,6] on the theory without a monopole term give energy histograms which indicate a first-order transition. The problem in these simulations is that the tunneling between the phases is strongly suppressed. In order to overcome the difficulty the authors of [5] introduce some type of iterative reweighting for different β, while the authors of [6] use a matching of hot and cold start results.

To reconsider the case with a monopole term is of interest in two respects. First the variation of the details of the transition with the weight of this term provides further insight into the properties of the theory. Second, if the strength of the transition turns out to decrease with this weight, then, by making the weight a dynamical variable, one can set up a very efficient simulation algorithm. The efficiency of such a procedure has been demonstrated in [7], where, by making the number of states q in the Potts model a dynamical variable, the authors could bridge the energy gap that occurs for $q > 4$.

Further aspects of the U(1) theory which deserve reconsideration are the properties of the spatial structure of the monopole currents in the configurations and their relationship to the global features showing up in the observables. First results along these lines have been presented some time ago by Grösch *et al.* [8]. Recently this issue has been addressed again by Bode *et al.* [9] who observed that in 4D compact U(1) theory one is confronted with clusters of monopole lines rather than with single loops.

Because the topological description is straightforward for loops only, this raises the question if a satisfactory topological characterization of networks of current lines can be found. In this context one should also discuss the work by Lang and Neuhaus [10], who, simulating the model on the surface of a 5D hypercube (homeormporphic to a four-sphere) rather than on a 4D lattice with periodic boundary conditions (corresponding to a torus), found that the first-order signal disappears.

In the present paper we show that the additional monopole term provides the features needed to set up a powerful simulation algorithm. Our investigations give detailed properties of the phase transition and their dependence on the weight of the monopole term. We introduce a topological characterization of networks of current lines and find that the topology of these networks signals the phases.

Section II gives definitions and general relations. In Sec. III, the method of the Monte Carlo simulations is described. Section IV presents the results based on histograms and a discussion of the phase structure. In Sec. V, the topological characterization of networks of current lines is outlined. In Sec. VI, the numerical results on current networks are presented and discussed. Section VII contains some conclusions.

II. ACTION AND MONOPOLE CURRENTS

The Wilson action supplemented by a monopole term is of form

$$S = \beta \sum_{\mu>\nu,x} (1 - \cos\Theta_{\mu\nu,x}) + \lambda \sum_{\rho,x} |M_{\rho,x}| \ . \qquad (2.1)$$

In terms of the link angles $\Theta_{\mu,x} \in [-\pi, \pi)$ the plaquette flux $\Theta_{\mu\nu,x} \in [-4\pi, 4\pi)$ is

$$\Theta_{\mu\nu,x} = \Theta_{\mu,x} + \Theta_{\nu,x+\mu} - \Theta_{\mu,x+\nu} - \Theta_{\nu,x} \ .$$

The physical flux $\bar{\Theta}_{\mu\nu,x} \in [-\pi, \pi)$ is defined [1] by

$$\Theta_{\mu\nu,x} = \bar{\Theta}_{\mu\nu,x} + 2\pi n_{\mu\nu,x} \ , \qquad (2.2)$$

where $n_{\mu\nu,x} = 0, \pm 1, \pm 2$. The monopole content of 3D cubes which enters the additional term in (2.1) is given by

$$2\pi M_{\rho,x} = \tfrac{1}{2}\epsilon_{\rho\sigma\mu\nu}(\bar{\Theta}_{\mu\nu,x+\sigma} - \bar{\Theta}_{\mu\nu,x}) \ , \qquad (2.3)$$

where $M_{\rho,x} = 0, \pm 1, \pm 2$. The $\bar{\Theta}_{\mu\nu,x}$ are invariant under gauge transformations

$$\Theta'_{\mu,x} = [\Theta_{\mu,x} + \chi_{x+\mu} - \chi_x + \pi] \bmod 2\pi - \pi$$

with $\chi \in [-\pi, \pi)$ (which guarantees that $\Theta'_{\mu,x} \in [-\pi, \pi)$ as well).

We find it convenient to introduce $J_{\rho,x} = M_{\rho,x+\rho}$ and $\vartheta_{\rho\sigma,x} = \frac{1}{2}\epsilon_{\rho\sigma\mu\nu}\bar{\Theta}_{\mu\nu,x+\rho+\sigma}$ because then the current conservation law

$$\sum_{\rho}(J_{\rho,x} - J_{\rho,x-\rho}) = 0 \qquad (2.4)$$

and the field equation

$$\sum_{\sigma}(\vartheta_{\rho\sigma,x} - \vartheta_{\rho\sigma,x-\sigma}) = 2\pi J_{\rho,x} \qquad (2.5)$$

have a straightforward geometric interpretation on the dual lattice.

Summing (2.5) over three of the four coordinates, for periodic boundary conditions we obtain

$$\sum_{x_{\mu_0} x_{\mu_1} x_{\mu_2}} J_{\mu_3,x} = 0 \ , \qquad (2.6)$$

i.e., the vanishing of the net current flow through any hypersurface perpendicular to the direction of the flow. We note that (2.4) holds separately on each network N of current lines (cf. Sec. V) disconnected from the rest. Therefore, summing (2.4) in that case over three of the four coordinates we still get

$$\sum_{x_{\mu_0} x_{\mu_1} x_{\mu_2}} J_{\mu_3,x} = f_{\mu_3} \ \text{ for } J_{\mu,x} \in \mathrm{N} \ , \qquad (2.7)$$

where f_{μ_3} is constant. By (2.6) the net current flows f_μ of the occurring networks have to sum up to zero.

III. METHOD OF SIMULATION

In the usual simulations λ is a fixed parameter and one deals with a probability distribution $\mu_\lambda(\Theta) = \exp[-S_\lambda(\Theta)]/Z_\lambda$. In order to make the parameter λ a dynamical variable we consider $\mu_\lambda(\Theta)$ as the conditioned probability to get a configuration Θ given a definite value λ and allow the values of λ to vary with a chosen probability distribution $f(\lambda)$. Then, to simulate the joint probability distribution $\mu(\Theta, \lambda) = f(\lambda)\mu_\lambda(\Theta)$, we use $\mu(\Theta, \lambda) = \exp[-S(\Theta, \lambda)]/Z$ with $S(\Theta, \lambda) = S_\lambda(\Theta) + g(\lambda)$. This implies that the relation between f and g is given by

$$f(\lambda) = Z_\lambda \exp[-g(\lambda)]/Z \qquad (3.1)$$

with $Z = \sum_\lambda Z_\lambda \exp[-g(\lambda)]$.

In the simulations we use a discrete set of n values of λ. For the efficiency of the simulations an appropriate choice of $f(\lambda)$ is crucial. We require this to be (approximately) constant so that (almost) identical total numbers of sweeps are spent at all values of λ. By (3.1), constant $f(\lambda)$ means $g(\lambda) = \ln Z_\lambda + c$, with an arbitrary constant c. Reasonable values of $g(\lambda)$ are readily obtained by short runs at fixed λ. These values can be improved iteratively in the full simulations, replacing $g(\lambda)$ by $g(\lambda) + \ln[nf(\lambda)]$ in subsequent iterations, which converges to constant $g(\lambda)$.

While the total amount of time spent at a definite λ value is fixed by $f(\lambda)$, there is still the freedom to vary the average stay time (the average number of sweeps spent at a particular λ before leaving it). The reciprocal of this time is the sum of the transition probabilities to the neighboring λ values. To get an efficient algorithm these probabilities must not be too small, which means that one must use a sufficient number of λ values. Further it appears appropriate to make these probabilities (roughly) the same in all cases, which can be achieved by adjusting the distances between the λ accordingly.

In our application of the algorithm each update of the Θ link variables has been followed by an update of λ. As individual update steps we have used Metropolis steps in both cases. For the λ_q with $q = 1, \ldots, n$ we have used the proposal matrix

$$\tfrac{1}{2}(\delta_{q+1,q'} + \delta_{q,q'+1} + \delta_{q,1}\delta_{q',1} + \delta_{q,n}\delta_{q',n}) \ .$$

For the efficiency of the algorithm it is crucial that the fact of making λ a dynamical variable opens an easier pathway between the phases. In the case under consideration this happens because the strength of the first-order transition decreases with λ. This is illustrated by Fig. 3 (discussed in Sec. IV), which indicates that traveling along the peaks is easier than tunneling through the valleys.

For each value of λ one must fix a corresponding value of β. To exploit the algorithm already at the stage when one searches for the transition line, the λ interval can be gradually extended, starting from a region with overlapping peaks and adjusting the β values with increasing statistics.

The tunneling times [14] between the phases for our algorithm with dynamical λ are greatly reduced as compared to those of a conventional Metropolis algorithm. For example, for $L = 8$ at the phase transition line (cf. Sec. IV) we get, in units of 10^3, 0.17(2) as compared to 3.0(3) for $\lambda = 0$ and 0.25(4) as compared to 23(5) for $\lambda = -0.3$.

Since we are interested in the results for all of the λ values considered, these times reflect the actual gain. If we were interested only in one of the λ values, to make a fair comparison we would have to multiply the times of our algorithm roughly by the number of λ values used. Thus envisaging interest in the results for $\lambda = -0.3$ only, multiplying the above timing by $n = 21$, we would find that there remains still considerable gain. Envisaging only $\lambda = 0$, where traveling to negative values is no longer needed, the factor would be 15 and there would be some gain there as well.

The actual point, however, is that for large L (in which one is mainly interested), and similarly also at negative λ, our algorithm is in any case superior. This occurs simply because then the peaks in the energy distribution related to the phases (cf. Sec. IV) get separated so that by using conventional algorithms one does not observe any transitions at all. It should be realized that the situation in this region is entirely different from the one in regions where there is considerable overlap of the peaks, in which case one can, of course, not gain much.

A further important virtue of the present algorithm is that it allows vectorization and parallelization of the computer programs (as does, e.g., not hold for the multicanonical method [11]). This has allowed us to develop an efficient parallel implementation running on the connection machine CM-5.

TABLE I. β_C of phase transition for $L = 8$; β and $g(\lambda)$ of simulations.

λ	β_C	β	$g(\lambda) - g(-0.3)$
−0.30	1.1786(1)	1.1785	$0.000\,00\times10^{0}$
−0.25	1.1501(1)	1.1501	1.74914×10^{2}
−0.20	1.1217(1)	1.1217	3.54865×10^{2}
−0.15	1.0932(1)	1.0932	5.40888×10^{2}
−0.10	1.0647(1)	1.0646	7.33197×10^{2}
−0.05	1.0361(1)	1.0361	9.30199×10^{2}
0.00	1.0075(1)	1.0074	1.13491×10^{3}
0.05	0.9787(1)	0.9788	1.34483×10^{3}
0.10	0.9496(1)	0.9498	1.56490×10^{3}
0.15	0.9203(1)	0.9205	1.79466×10^{3}
0.20	0.8908(1)	0.8909	2.03454×10^{3}
0.25	0.8609(1)	0.8610	2.28503×10^{3}
0.30	0.8304(1)	0.8306	2.54875×10^{3}
0.35	0.7995(1)	0.7998	2.82532×10^{3}
0.40	0.7680(1)	0.7685	3.11653×10^{3}
0.45	0.7359(1)	0.7364	3.42644×10^{3}
0.50	0.7028(1)	0.7034	3.75730×10^{3}
0.525	0.6860(1)	0.6864	3.93287×10^{3}
0.55	0.6688(2)	0.6693	4.11274×10^{3}
0.575	0.6512(2)	0.6515	4.30418×10^{3}
0.60	0.6335(2)	0.6337	4.49916×10^{3}

In the present work we have run the algorithm with dynamical λ for $L = 8$ using the 21 values of λ, and corresponding values of β and $g(\lambda)$, given in Table I. For $L = 8$ at $\lambda = 0.9$ and for $L = 16$ at $\lambda = 0$ and at $\lambda = 0.6$ we have also performed conventional simulations at a number of β values. The statistics we collected is larger than 10^5 sweeps for each of the λ values we considered for $L = 8$ as well as for $L = 16$.

IV. PHASE STRUCTURE

Rather precise results on the phase transition have recently been obtained [5,6] in the absence of a monopole term by considering energy histograms. Including the monopole term in investigations based on histograms, we find that the strength of the first-order transition decreases as λ increases. This is seen from Fig. 1, which compares the distributions $P(E)$ of the average plaquette energy

$$E = (1/6L^4) \sum_{\mu>\nu,x} (1 - \cos\Theta_{\mu\nu,x})$$

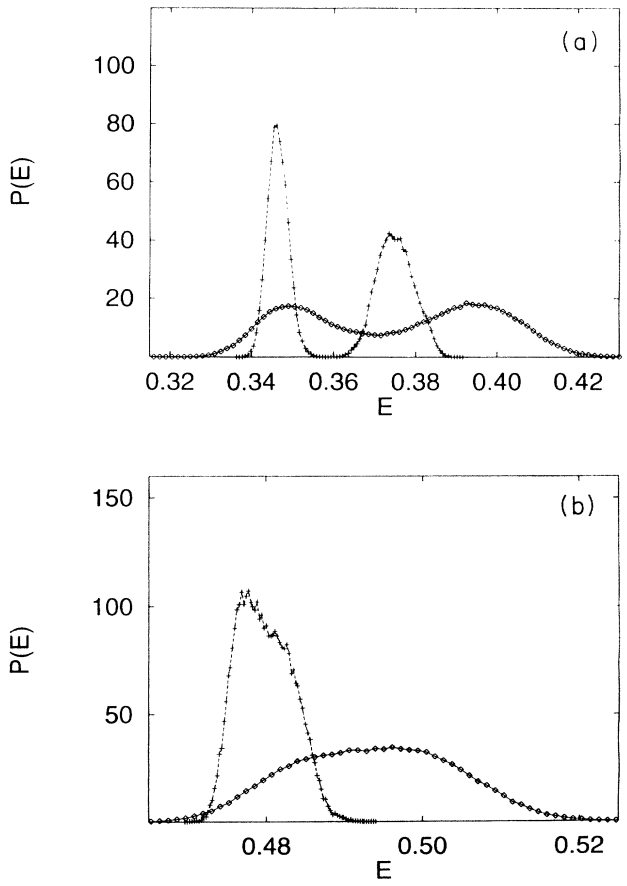

FIG. 1. Distribution $P(E)$ in the transition region on lattices with $L = 8$ (rhombs) and $L = 16$ (crosses), (a) for $\lambda = 0$ and (b) for $\lambda = 0.6$.

on lattices of sizes $L = 8$ and 16 for $\lambda = 0$ and 0.6. (The data of Fig. 1 for $L = 8$ are given in Table I. For $L = 16$ we used $\beta = 1.010\,781$ for $\lambda = 0$ and $\beta = 0.6428$ for $\lambda = 0.6$. For $L = 16$ and $\lambda = 0$ the peaks have been obtained by equal numbers of hot and cold starts, respectively.)

As the peaks overlap the determination of the location of the phase transition needs special care. This is illustrated by Fig. 2, which for $\lambda = 0.6$ and $L = 16$ shows the sensitivity to the value of β.

From Fig. 3, which presents the distribution $P(E, \lambda)$ we obtained in the transition region for $L = 8$ by simulations with dynamical λ, the decrease of the strength of the transition is seen in more detail. The figure also makes the case for our algorithm: from the profile of the distribution it is clear how a simulation with dynamical λ can trace the peaks and thus avoid the long correlation times due to the separation of the phases in the region where the transition is strongly of the first order.

We define as location of the phase transition the maximum of the specific heat, which determines for us β_C for given λ. To adjust the data measured in the transition region appropriately, we use reweighting [15]. The location of the transition in (β, λ) space is depicted in Fig. 4 for $L = 8$. Corresponding numerical values of β_C up to $\lambda = 0.6$ are given in Table I. For $L = 8$ at $\lambda = 0.9$ we get $\beta_C = 0.3885(5)$ and for $L = 16$ at $\lambda = 0.6$ we obtain $\beta_C = 0.6428(3)$; the value for $L = 16$ at $\lambda = 0$ determined in Ref. [6] is $\beta_C = 1.010\,82(6)$.

Figure 5 presents the latent heat as a function of λ at the phase-transition line for $L = 8$, confirming the fact, already seen from Fig. 1 for $L = 8$ and 16 and from Fig. 3 for $L = 8$ for a whole range of λ values, that the strength of the transition decreases with increasing λ. We give the data in Fig. 5 up to the point where separation of phases appears numerically justified. The merging of the peaks signals that the transition ultimately gets of second order (a further indication of this will be discussed in Sec. VI).

We confirm the observation [6] for $\lambda = 0$ that the latent heat at the transition point from $L = 8$ to 16 decreases. However, the requirement for a first-order transition is

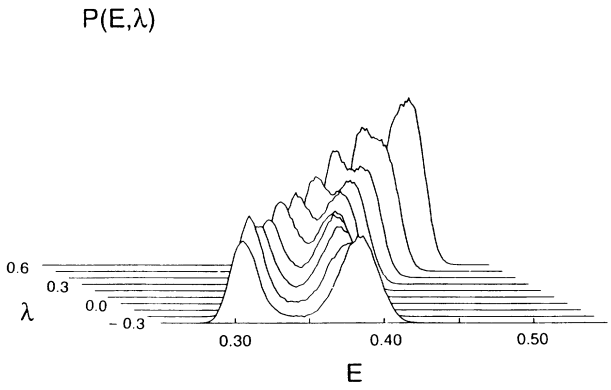

FIG. 3. Distribution $P(E, \lambda)$ for $L = 8$ with β in the transition region.

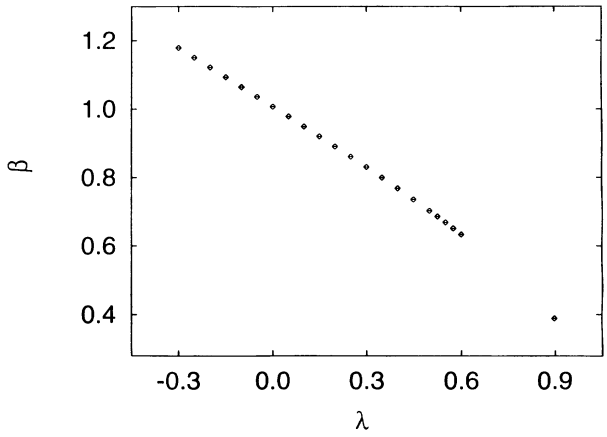

FIG. 4. Location of phase transition in (β, λ) space for $L = 8$, β versus λ.

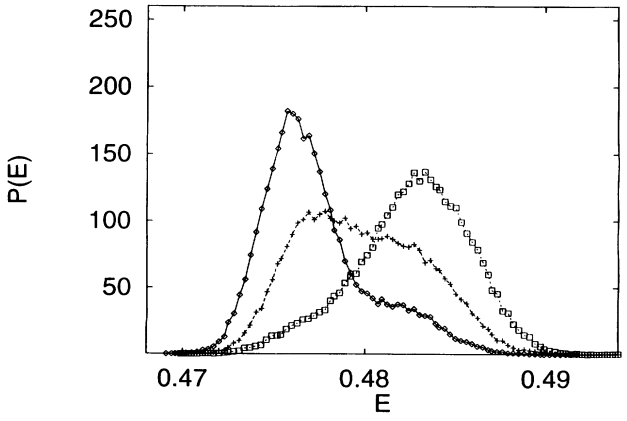

FIG. 2. Distributions $P(E)$ for $\lambda = 0.6$ and $L = 16$, for $\beta = 0.6432$ (rhombs), $\beta = 0.6428$ (crosses), $\beta = 0.6424$ (squares).

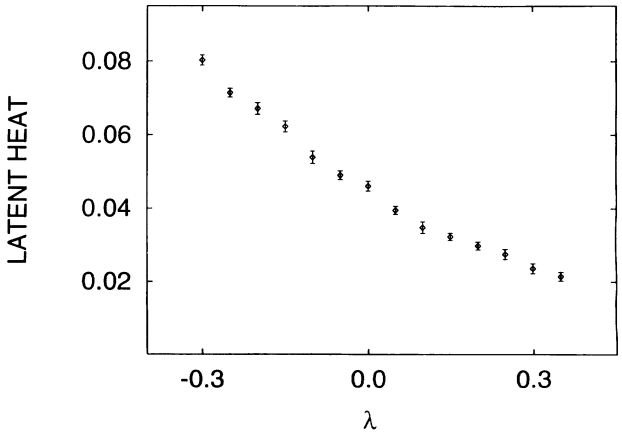

FIG. 5. Latent heat for $L = 8$ as function of λ at the transition line.

only that extrapolation to infinite L of the latent heat versus $1/L$ leads to a finite value [12]. For the Potts model it has recently been demonstrated that such an extrapolation does reproduce known results [13]. If we extrapolate our values 0.046(2) for $L = 8$ and 0.030(2) for $L = 16$ linearly versus $1/L$ we obtain the finite value 0.014. It is, nevertheless, still an open question to what extent finite-size scaling already applies.

Our results for the distributions of the monopole number density $\rho = (1/4L^4)\sum_{\rho,x}|M_{\rho,x}|$ are very similar to the ones presented above for the distributions of the plaquette energy E. This confirms the strong correlation between E and ρ at the transition point which has been known for some time [16]. In Fig. 6, which illustrates data obtained with $L = 8$ and $\lambda = -0.3$, we show the preferred direction of the distribution $P(E,\rho)$ in (E,ρ) space. From Fig. 7, which exhibits $P(E,\rho)$ for $L = 8$ and $\lambda = -0.3$, 0, 0.3, 0.6, 0.9, it is seen that the slope of the correlation shows only little dependence on λ. In addition from Fig. 7 it is apparent that the ρ of the cold phase is roughly the same for all λ.

From Fig. 7 we see that the slope of the correlation between plaquette energy and monopole density $\Delta E/\Delta\rho$ ranges from approximately 1.1 to approximately 1.3, with the smaller value slightly favored for larger monopole density. Remembering that the ratio between total numbers of plaquettes and cubes in a four-dimensional lattice is $\frac{3}{2}$, this indicates that the average total extra plaquette energy associated with the presence of a monopole is $\Delta E_{\rm tot} \approx 1.8$. A semiclassical explanation for this number can be obtained along the following lines. A calculation of the minimal plaquette energy needed to produce a monopole loop of length 4 in an otherwise totally ordered field configuration gives $E = 6.65$, i.e., a total plaquette energy per monopole ≈ 1.61. (We have used a constrained relaxation technique to evaluate this number. One must of course impose a constraint since a monopole loop is classically unstable.) This can account for the value of $\Delta E/\Delta\rho$ in the low monopole density regime.

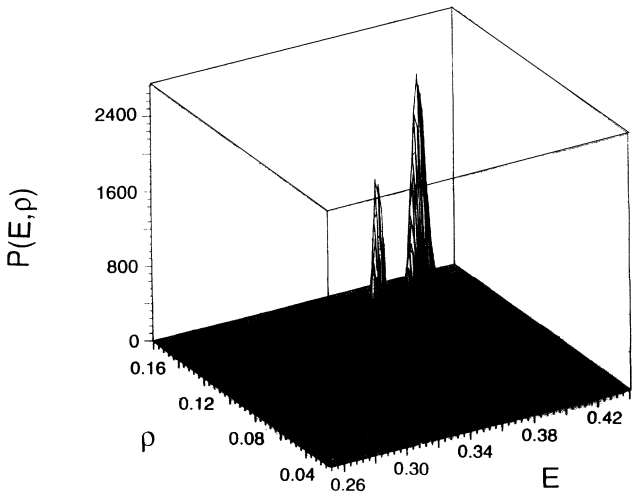

FIG. 6. Distribution $P(E,\rho)$ for $L = 8$ and $\lambda = -0.3$ in the transition region.

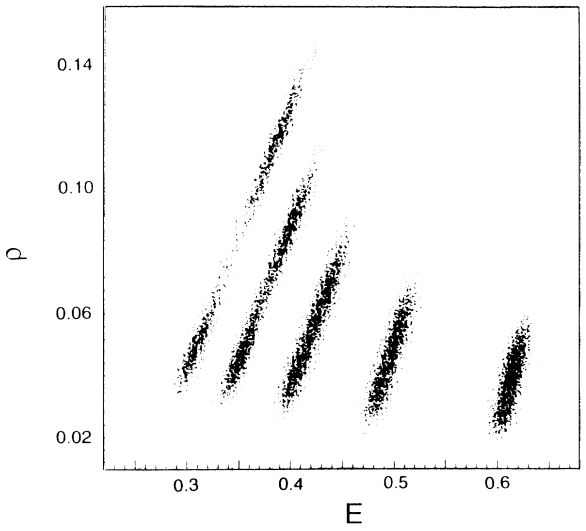

FIG. 7. $P(E,\rho)$ for $L = 8$ in the transition region, for $\lambda = -0.3$, 0, 0.3, 0.6, 0.9 (giving the distributions from left to right, respectively).

With a very high density of monopoles a more appropriate quantity to consider would be the total plaquette energy necessary to produce a long monopole line. In this case the plaquette energy per monopole can be obtained by calculating the total plaquette energy for a single monopole configuration in a three-dimensional system, which is given by $E = 4.41$. This number is much larger than the observed $\Delta E/\Delta\rho$, but one must also consider that in regimes of high monopole densities the monopoles are produced over the background of a rather disordered gauge field. Thus it would not seem correct to attribute to the presence of a monopole the entire energy necessary to create it from the vacuum, but instead only the excess energy over the background. For this reason we have also calculated the excess plaquette energy above some definite cutoff in a classical monopole configuration [i.e., we have summed $\min(E_{\rm plaquette} - E_{\rm cutoff}, 0)$ over all plaquettes]. With $E_{\rm cutoff} = 0.2$ and 0.25 this gives $E = 1.80$, and 1.50, respectively. Thus, in either case (low and high density of monopoles) the number that emerges from the semiclassical calculation is in reasonable agreement with the observed values.

V. CHARACTERIZATION OF NETWORKS

The currents $J_{\rho,x}$ related to links of the dual lattice take the values $0, \pm 1, \pm 2$. We define current lines such that for $J_{\rho,x} = 0$ there is no line on the link, for $J_{\rho,x} = \pm 1$ there is one current line in the positive or negative direction, respectively, and for $J_{\rho,x} = \pm 2$ there are two lines in the positive or negative direction. Because the $J_{\rho,x}$ are subject to (2.4) the same number of lines must arrive at and depart from a site.

The current lines thus form connected sets which we call networks. The topologically relevant ingredients of

these networks are the vertices, defined as the sites where at least two lines arrive (and depart), and the edges, defined as the current lines connecting the vertices.

For networks of current lines it is intuitively clear whether a network wraps around the torus in some direction or not. However, a precise mathematical criterion remains to be given. It should be obvious that cutting the network into loops is not allowed because (apart from being highly nonunique) this would change the topology. In the following we point out how the fundamental homotopy group π_1 can be used to obtain the desired topological characterization.

The elements of π_1 correspond to equivalence classes of paths which can be deformed continuously into each other and which all start and end at the same point, called base point. A strategy to determine $\pi_1(\mathbb{X}, b)$ of a space $\mathbb{X}$ with a base point b is to cover $\mathbb{X}$ by a suitably dense network and to make use of the fact that the related edge path group is isomorphic to π_1 [17]. Analyzing the network then leads to $\pi_1(\mathbb{X}, b)$. For the four-dimensional torus considered here one gets $\pi_1(\mathbb{T}^4, b) = \mathbb{Z}^4$ independently of the choice of b.

This motivates a related procedure which we propose for characterizing the topology of the networks of current lines embedded in $\mathbb{T}^4$. For a particular network N it exploits the observation that the analysis provides the generators of $\pi_1(\mathbb{T}^4, b)$ if $\mathbb{T}^4$ is suitably covered by N, while it gives only those of a subgroup thereof if N does not wrap around in all directions. Thus one gets an appropriate characterization by the (proper or improper) subgroup associated with N.

To derive our rules we choose one vertex point of N to be the base point b and consider the set of all loops through b, i.e., of all paths through N which start and end at this point. We then use the fact that the group content of this set is not changed if we perform mappings preserving the homotopy of all of these paths. This in particular holds for a mapping by which one edge shrinks to zero length. By a sequence of such mappings one finally can shift all other vertices to b. One thus gets a bouquet of paths starting and ending at the base point.

To perform this shrinking procedure in practice, we represent any path on $\mathbb{T}^4$ by a vector which is the sum of the oriented steps along the path. Thus a vector of this type is associated with each edge (and depends on the starting point and the end point of the edge, however, not on the particular path it takes). Then a shrinking of one edge implies that the coordinates of the moving vertex and the vectors of all other edges connected to this vertex are to be modified appropriately.

For a network N with K_0 vertices and K_1 edges one obtains a bouquet of $K = K_1 - K_0 + 1$ loops on $\mathbb{T}^4$, which are related to elements of $\pi_1(\mathbb{T}^4, b)$. The bouquet is described by a set of vectors of the type introduced above, $\mathbf{s}_i$ with $i = 1, \ldots, K$. If the ith loops wind around the torus w_{ij} times in direction j (including the sign), the jth component of the respective vector is $s_{ij} = w_{ij} L_j$ where L_j denotes the lattice size and $j = 0, 1, 2, 3$. Thus, one can equivalently use the vectors $\mathbf{w}_i$ with components w_{ij} to represent the bouquet.

The networks considered here have the additional properties of given path orientation and of respecting current conservation at the vertices. This reduces the allowed patterns. For the net current flow (2.7) it implies the relation $\mathbf{f} = \sum_i \mathbf{w}_i$ for the bouquet vectors, which restricts the form of the bouquet matrix.

While the group content of the bouquet is unique, which particular loops occur depends on the succession of the shrinking mappings chosen to form the bouquet. Transformations between equivalent bouquets have to preserve homotopy and to respect current conservation. We observe that elementary maps of this type are ones in which three vectors $\mathbf{w}_a, \mathbf{w}_b, \mathbf{w}_c$, selected out of the bouquet, are replaced by $\mathbf{w}_a$, $\mathbf{w}_b - \mathbf{w}_a, \mathbf{w}_c + \mathbf{w}_a$ (as one readily verifies considering the partial network with two vertices from which, depending on the edge selected for shrinking, the first or the second form arises).

Obviously these elementary maps correspond to steps of a modified Gauss elimination procedure within the bouquet matrix w_{ij}, in which adding of a row to another one requires to subtract it simultaneously from a further row. Applying steps of this type w_{ij} can be cast into a standard from with rows $\mathbf{a}_1, \ldots, \mathbf{a}_r, \mathbf{t}, \mathbf{0}, \ldots, \mathbf{0}$ where $\mathbf{a} \neq \mathbf{0}$ and where $r \leq 4$ is minimal. Because the entries of the matrix are integers and because divisions are not allowed in the procedure, one in general remains with a triangular form of the $\mathbf{a}_i$, for $r = 4$ with i elements which may differ from zero (while in our application except for very few cases further reduction to $a_{ij} = \pm\delta_{ij}$ occurs).

The pair form with rows $\mathbf{a}_i, -\mathbf{a}_1, \ldots, \mathbf{a}_r, -\mathbf{a}_r, \mathbf{f}, \mathbf{0}, \ldots, \mathbf{0}$, which explicitly exhibits $\mathbf{f}$, for $K \geq 2r + 1$ is immediately obtained from the standard form. For $\mathbf{f} = \mathbf{0}$ the number of nontrivial directions is r. For $\mathbf{f} \neq \mathbf{0}$, rewriting the pair form for $K \geq 2r + 3$ as $\mathbf{a}_1, -\mathbf{a}_1, \ldots, \mathbf{a}_r, -\mathbf{a}_r, \mathbf{f}, -\mathbf{f}, \mathbf{f}, \mathbf{0}, \ldots, \mathbf{0}$, it is seen that the number of independent pairs out of $\mathbf{a}_1, -\mathbf{a}_1, \ldots, \mathbf{a}_r, -\mathbf{a}_r, \mathbf{f}, -\mathbf{f}$ is the number of nontrivial directions, which may be r or, provided that $r+1 \leq 4$, also $r + 1$.

VI. MONOPOLE CURRENTS

There exist quite a number of contacts of current lines. We define their number at a site by the number of lines arriving at the site (or, equivalently, departing from it) minus one. We find that their overall number per size is larger in the hot phase than in the cold one, decreases with increasing λ, and shows little dependence on L. The data in Table II give an overview of this.

The number of contacts in a network equals the number of links along its lines minus the number of sites on its lines. We get a roughly linear increase of the number of contacts with the size of a network (with some increase of the fluctuations around the curve and of its slope with size). For $\lambda = 0$ this confirms an observation of Ref. [9]. For larger λ we find that the slope gets smaller. We see almost no L dependence of the slopes. Table II also contains mean numbers of contacts in a network per network size (for networks larger than 19), which are seen to be similar to the overall numbers.

In Fig. 8(a), we depict the probability to find a net-

TABLE II. Contacts per size in units of 100.

L	λ	Phase	Overall	Network
8	−0.3	Cold	6.2(1)	9.7(2)
		Hot	11.3(1)	11.7(2)
8	0.0	Cold	5.5(1)	8.4(1)
		Hot	7.9(1)	8.7(1)
8	0.3	Cold	4.4(1)	6.7(1)
		Hot	5.9(1)	7.0(1)
8	0.6		3.9(1)	5.6(1)
8	0.9		3.0(1)	4.5(1)
16	0.0	Cold	5.1(1)	8.2(1)
		Hot	7.1(1)	8.2(1)
16	0.6		3.4(1)	5.5(1)

work which is nontrivial in at least one direction and in Fig. 8(b) the probability to find one nontrivial in four directions as functions of λ along the transition line for $L = 8$. We have obtained the data for the hot (confining) and the cold (Coulomb) phase by separating the E histogram at the minimum between the peaks (up to the λ value where this has been still possible). From Fig. 8 it is obvious that the topological characterization provides a signal for the phases.

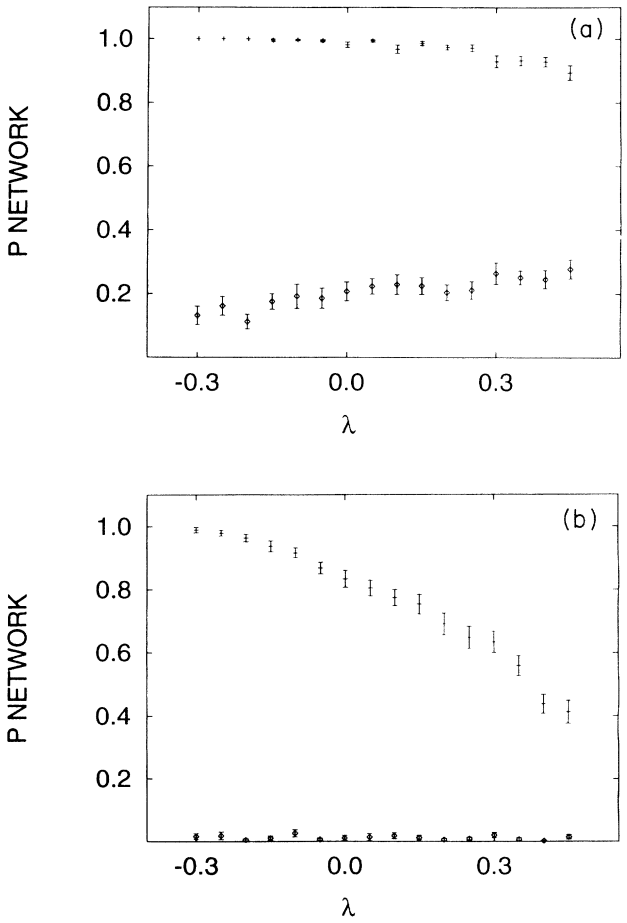

FIG. 8. Probability for a network in cold (rhombs) and hot (crosses) phase as function of λ for $L = 8$, (a) being nontrivial in at least one direction, (b) being nontrivial in four directions.

We find that for $L = 16$ this effect at $\lambda = 0$ is already more pronounced than it is for $L = 8$ at $\lambda = -0.3$. The obvious reason for this is that the peaks related to the phases become well separated, which makes the signal for the phases rather perfect, the hot phase being indicated by a network nontrivial in all directions, and the cold one by the absence of nontrivial networks. This appears to be the generic situation for larger lattices. It thus turns out that the topological characterization provides an unambiguous signal for the phases.

It is useful to emphasize the difference between the topological classification of the networks we have given here and the "winding number" $(1/L_\mu)\sum_{x\in\mathbb{N}} M_{\mu,x}$, as defined in Ref. [9], which, because of current conservation, equals the net current flow f_μ (2.7). Our topological characterization formalizes the intuitive notion that a network of monopole loops wraps all around the torus, i.e., that it contains oriented paths that allow one to go around the torus and come back to the original point. This can happen, and thus give to the network a nontrivial topology, even if the network carries no net current flow. Indeed, for $\lambda = 0$ we also found numerically that the net current flow is nonzero only in very rare cases for $L = 8$ and not at all for $L = 16$. For larger λ the fraction of such events increases. Some of our data on the net current flow are reproduced in Table III.

Because of (2.6) $f_\mu \neq 0$ implies that more than one nontrivial network occurs. From Table III it is seen that the case $\mathbf{f} \neq \mathbf{0}$ coincides indeed with the occurrence of more than one nontrivial network. It also shows that the number of these networks increases with λ.

In Fig. 9, we present the probability to find networks being nontrivial in 0 to 4 directions as function of λ along the transition line (without separating phases and thus allowing to cover the full range of λ). For trivial networks within errors there is no dependence on λ. The fraction of nontrivial networks being nontrivial in less than four directions is seen to increases with λ. Thus there is a λ region where all of these structures become similarly important, which is a further indication of the transition getting of second order.

Figure 10 shows the mean size of the largest network for $L = 8$ as function of λ along the transition line (the statistical errors given are small as compared to the fluctuations of sizes around the mean). The signal for the

TABLE III. Probability for $\mathbf{f} \neq \mathbf{0}$ and for more than one nontrivial network in units of 100.

L	λ	$\mathbf{f} \neq \mathbf{0}$	No. =2	No. =3	No. =4
8	−0.3	0.6(4)	0.6(4)	0.0(2)	0.0(2)
	0.0	1.6(5)	1.6(5)	0.0(2)	0.0(2)
	0.3	6.6(1.3)	6.6(1.3)	0.0(2)	0.0(2)
	0.6	14.6(1.5)	12.7(1.5)	1.4(4)	0.5(3)
	0.9	19.3(3.3)	15.9(2.7)	3.0(5)	0.4(3)
16	0.0	0.0(3)	0.0(3)	0.0(3)	0.0(3)
	0.6	12.0(2.7)	12.0(2.7)	0.0(3)	0.0(3)

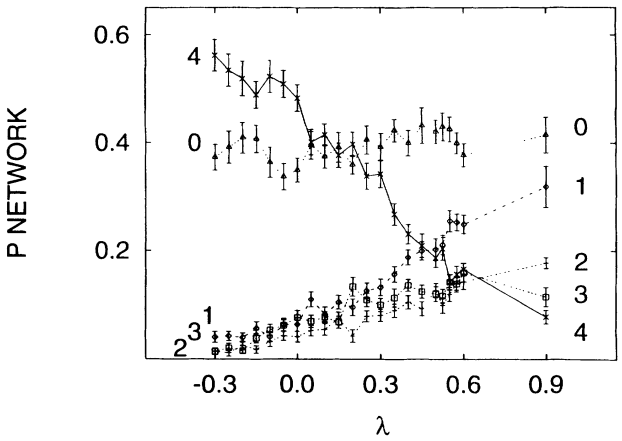

FIG. 9. Probability for a network being nontrivial in 0–4 directions as a function of λ for $L = 8$.

phases is similar as in Fig. 8, which reflects the fact that the nontrivial network is large. Our data for $L = 16$ show the same effect [for $\lambda = 0$ the mean size of the largest network in the hot phase is 12 900(200) and in the cold phase it is 790(50)]. Figure 10 in addition reveals that only the hot phase data change significantly with λ (as can also be observed for ρ in Fig. 7).

Figure 11 gives the average number $N(l)$ of trivial networks as a function of their size l for $L = 16$ and $\lambda = 0$ in the transition region. The hot and cold phase data turn out to be rather similar. The distributions within errors decrease with power laws, slightly faster for the hot phase. The plots for the $L = 8$ data look very similar, apart from the numbers being smaller. They show very little dependence on λ. Table IV, with the results of a fit of $N(l)$ versus kl^{-z}, summarizes these findings.

The power law $N(l) \sim l^{-z}$ may be related to a fractal dimension D_f. Assuming that the sum of lengths of networks of size l per volume, $lN(l)/V$, does not change under coarse graining, by which it gets the form $(l/b^D f)N(l/b^D f)/(b^D V)$, one obtains $z = 1 + D/D_f$. Inserting z from Table IV and $D = 4$ it follows that D_f is in the range between 1.8 and 2.8, i.e., well below 4.

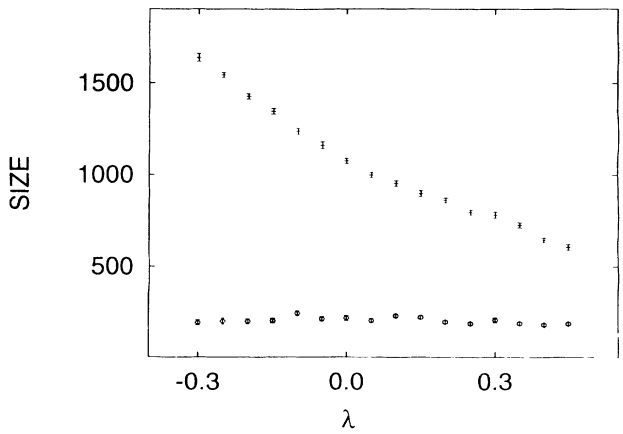

FIG. 10. Mean size of largest network in cold (rhombs) and hot (crosses) phase as function of λ for $L = 8$.

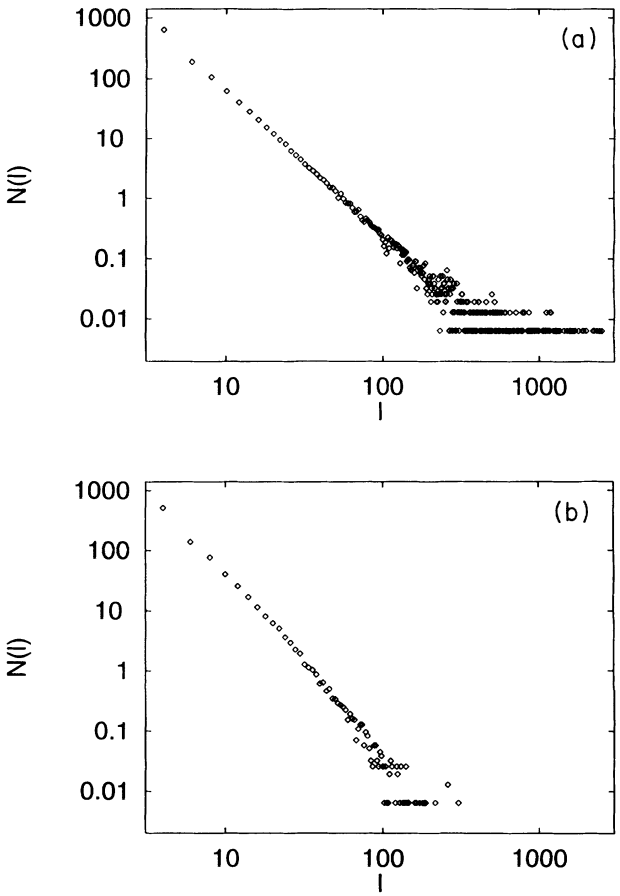

FIG. 11. Number $N(l)$ of trivial networks as function of size l for $L = 16$ and $\lambda = 0$, (a) cold phase, (b) hot phase.

Our observations can be used to get insight into the mechanisms involved in the phase transition. We have noticed (cf. Figs. 7 and 10) that in the cold phase ρ and the size of the largest network show little dependence on λ, while in the hot phase these quantities decrease strongly with λ. The decrease of the latent heat (cf.

TABLE IV. z and k from fits kl^{-z} to the probability for trivial networks of size l.

L	λ	Phase	z	k
8	−0.3	Cold	2.46(2)	1 164(42)
		Hot	3.22(3)	2 059(110)
8	0.0	Cold	2.48(2)	1 168(27)
		Hot	3.01(2)	1 814(60)
8	0.3	Cold	2.48(2)	995(3)
		Hot	2.87(2)	1 494(43)
8	0.6		2.66(1)	1 158(21)
8	0.9		2.65(2)	1 007(36)
16	0.0	Cold	2.41(1)	15 430(130)
		Hot	2.85(1)	25 830(180)
16	0.6		2.63(1)	19 710(250)

Figs. 1, 3, and 5), due to the strong correlation between E and ρ (apparent from Figs. 6 and 7) essentially only reflects the indicated behavior of ρ. We have also seen that for trivial networks neither the distribution of their sizes (cf. Table IV) nor the probability to find them (cf. Fig. 9) show significant changes with λ. Therefore, the quantity most affected by λ must be the probability for the occurrence of nontrivial networks in the hot phase.

Thus the following picture emerges. For negative λ, there is typically one large nontrivial network in the hot phase. With increasing λ (and with the consequent suppression of monopoles) there occurs a progressive thinning of such network, which reduces its size and the value of ρ. Then increasingly it subdivides (Table III and Fig. 9) and breaks into smaller pieces. The dynamics at fixed λ may be illustrated in the following way. If there is a very large nontrivial network, it will tend to thin out to reach the size favored by the Boltzmann weight. On the torus it can, however, only get gradually smaller to a minimal size beyond which it must break into pieces. One possible explanation of the first-order nature of the transition for small λ would then be that, in the absence of thinning, the probability for the network to break up is low and a substantial amount of energy is also required. Therefore one gets the valley in the two-peak distribution and a gap.

If instead of the torus $\mathbb{T}^4$ one considers the sphere $\mathbb{S}^4$, because $\pi_1(\mathbb{S}^n)$ for $n \geq 2$ only contains the neutral element, the topological characterization no longer identifies distinct phases. To illustrate the dynamics in that case one may again consider a very large network. Now it can gradually get smaller without the above necessity to break at some point. Thus there should be only one peak (located roughly in the middle of the two-peak structure of a comparable torus).

The authors of Ref. [10], which simulate the system on the surface of a five-dimensional cube, homeomorphic to $\mathbb{S}^4$, observe indeed only one peak. Some caution apears appropriate, however, because on smaller lattices the inhomogeneities of the cube may cause smearing effects, that only the narrowing of the peak for larger systems would exclude.

However appealing, the topological interpretation of the order of the transition on the torus must face the notion that first-order transitions are bulk effects, in which boundaries play no role. In view of our observation that for increasing lattice size the topological characterization gets very clear, the disappearance of the transition also on extremely large lattices is hard to imagine. If one wishes to exclude the relevance of the boundary conditions then the interpretation of our observations on the topological properties of the networks would be that, although not crucial for the order of the transition, they form an excellent diagnostic tool. They indicate the occurrence of some type of percolation transition, whereby the monopole loops condense into a network pervading all of (four-dimensional) space. Also, the discrepancy of the results of [10] with such picture would remain to be explained. If the topological properties of the networks are, instead, intimately connected to the nature of the transition, this raises the question if such transitions, which certainly are of interest in models, could have physical implications, too.

VII. CONCLUSIONS

Adding a monopole term to the action has allowed us to set up a powerful simulation algorithm, to study the extended theory, and to extract the underlying mechanisms of the phase transition. We have found that the strength of the first-order transition decreases with the weight of the added terms in such a way that the transition ultimately gets of second order. We have presented detailed data on the properties of the system in this context. In order to be able to analyze the occurring configurations appropriately, we have worked out the topological characterization of networks of current lines. From our analysis we have obtained detailed results on these networks. In particular, we have found that their topological properties signal the phases.

ACKNOWLEDGMENTS

One of us (W.K.) wishes to thank the Physics Department of Boston University for kind hospitality during his visits. He also thanks Thomas Kerler for helpful discussions on topology. This work has been supported in part by the Deutsche Forschungsgemeinschaft through Grants Nos. Ke 250/7-1, 7-2, 9-1, and 11-1 and by the United States Department of Energy under Grant No. DE-FG02-91ER40676. The computations have been done on the CM5 of the Center for Computational Science of Boston University and since recently also on the CM5 of the GMD at St. Augustin.

[1] T. DeGrand and D. Toussaint, Phys. Rev. D **22**, 2478 (1980).

[2] J. S. Barber, R. E. Schrock, and R. Schrader, Phys. Lett. **152B**, 221 (1985).

[3] J. S. Barber and R. E. Schrock, Nucl. Phys. **B257**, 515 (1985).

[4] V. G. Bornyakov, V. K. Mitrujushkin, and M. Mueller-Preussker, in *Lattice '92*, Proceedings of the International Symposium, Amsterdam, The Netherlands, edited by J. Smit and P. van Baal [Nucl. Phys. B (Proc. Suppl.) **30**, 587 (1993)]; Berlin University Report No. IEP-92/5, 1992 (unpublished).

[5] V. Azcoiti, G. Di Carlo, and A. F. Grillo, Phys. Lett. B **267**, 101 (1991).

[6] G. Bhanot, T. Lippert, K. Schilling, and P. Ueberholz, Nucl. Phys. **B378**, 633 (1992); Int. J. Mod. Phys. C **3**, 1109 (1992).

[7] W. Kerler and A. Weber, Phys. Rev. B **47**, 11 563R

(1993).
[8] V. Grösch, K. Jansen, J. Jersak, C. B. Lang, T. Neuhaus, and C. Rebbi, Phys. Lett. **162B**, 171 (1985).
[9] A. Bode, T. Lippert, K. Schilling, and P. Ueberholz, in *Proceedings of the Conference on Large Scale Computational Physics on Massively Parallel Computers*, Jülich, Germany, 1993, edited by H. Herrmann and F. Karsch (World Scientific, Singapore, 1993); A. Bode, T. Lippert, and K. Schilling, in *Lattice 93*, Proceedings of the International Symposium, Dallas, Texas, edited by T. Draper *et al.* [Nucl. Phys. B (Proc. Suppl.) **34**, 549 (1994)].
[10] C. B. Lang and T. Neuhaus, in *Lattice 93* [9] [Nucl. Phys. B (Proc. Suppl.) **34**, 543 (1994)].
[11] B. A. Berg and T. Neuhaus, Phys. Lett. B **267**, 249 (1991); Phys. Rev. Lett. **68**, 9 (1992).
[12] J. Lee and J. L. Kosterlitz, Phys. Rev. Lett. **65**, 137 (1990); Phys. Rev. B **43**, 3265 (1991).
[13] W. Janke, Phys. Rev. B **47**, 14 757 (1993).
[14] A. Billoire, R. Lacaze, A. Morel, S. Gupta, A. Irbäck, and B. Petersson, Nucl. Phys. **B358**, 231 (1991); W. Janke, B. A. Berg, and M. Katoot, *ibid.* **B382**, 649 (1992).
[15] A. M. Ferrenberg and R. H. Swendsen, Phys. Rev. Lett. **61**, 2635 (1988).
[16] J. S. Barber, Phys. Lett. **147B**, 330 (1984).
[17] E. H. Spanier, *Algebraic Topology* (McGraw-Hill, New York, 1966); J. J. Rotman, *An Introduction to Algebraic Topology* (Springer, New York, 1988).

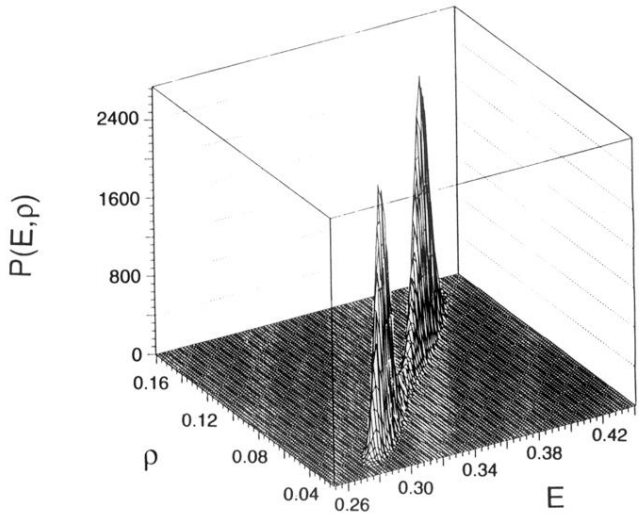

FIG. 6. Distribution $P(E, \rho)$ for $L = 8$ and $\lambda = -0.3$ in the transition region.